Biointerface Research in Applied Chemistry
Open-Access Journal (ISSN: 2069-5837)

*Article*
**Volume 13, Issue 5, 2023, 462**
https://doi.org/10.33263/BRIAC135.462

# Biogenic Synthesis of *Alternanthera Sessilis* Titanium Dioxide Nanoparticles (AS@$TiO_2$NP's): A Potential Contender against Perilous Pathogens and Catalytic Degradation of Organic Dyes

**Madathil Sowmya [1,*], Ananda Agasanapura Puttaswamy [1], Honnegowdanahalli Shivabasappa Nagendra Prasad [2], Natesan Geetha [3], Shanmugam Girija [5,*], Perumal Venkatachalam [1,4]**

1 Research and Development Centre, Bharathiar University, Coimbatore-641 046, Tamil Nadu, India
2 Department of Chemistry, Sri Jayachamarajendra College of Engineering, JSS Science and Technology University, Mysuru-570 006, Karnataka, India
3 Department of Botany, Bharathiar University, Coimbatore-641 046, Tamil Nadu, India
4 Department of Biotechnology, Periyar University, Salem-636011, Tamil Nadu, India
5 Department of Biotechnology, Bharathiar University, Coimbatore-641 046, Tamil Nadu, India
* Correspondence: genesumi@gmail.com(M.S.),girijabiotech@yahoo.co.in (S.G.);

Scopus Author ID

**Received: 24.08.2022; Accepted: 4.10.2022; Published: 24.12.2022**

**Abstract:** In the present investigation, *Alternanthera sessilis* titanium dioxide nanoparticles (AS@$TiO_2$NP's) were synthesized using tissue-culture grown plant leaves aqueous extracts of *A. asessilis* by the microwave irradiation method. The synthesized nanoparticles showed potential antibacterial activity and dye degradation properties. The synthesized AS@$TiO_2$NP's were amply characterized by using UV-visible spectroscopy, Fourier transform infrared spectroscopy (FT-IR), X-Ray diffraction (XRD), Scanning electron microscopy (SEM) and Energy dispersive X-Ray analysis (EDX). The probable functional bioactive compounds that were involved in capping on the surface of titanium nanoparticles were identified by FT-IR analysis. The presence of predominant peaks of $TiO_2$ 2θ value confirms the polycrystalline nature of the synthesized AS@$TiO_2$NP's. SEM analysis showed the crystalline structure of the synthesized AS@$TiO_2$NP's and the size of 69 nm with a zeta potential of 6.5 mV. The stability of AS@$TiO_2$NP's was studied with respect to pH, temperature, and salinity. The antibacterial potency of AS@$TiO_2$NP's was studied against *Staphylococcus aureus*, *Bacillus cereus*, *Escherichia coli*, and *Pseudomonas aeruginosa* compared to standard streptomycin drug and further validated with bacterial cell membrane damage by SEM analysis. The results of this experiment strongly suggest that the AS@$TiO_2$NP's could be effectively used as an alternate candidate for efficient and safe removal of toxic organic pollutants and can serve as a potential nanodrug towards bacterial inactivation and biofilm inhibition. The AS@$TiO_2$NP's showed good nature of biocompatibility at the hemostatic condition and insignificant cytotoxicity against 3T3L1 normal cell lines and significant antiproliferation activity to cancerous triple negative MDAMP231 cell lines compared to standard drug doxorubicin. The AS@$TiO_2$NP's are the potential candidate in the near future for bio-medication and industrial wastewater treatment.

**Keywords:** *Alternanthera sessilis*; antibacterial activity; dye degradation; biofilm and cytotoxicity.

## 1. Introduction

Nanotechnology is an emerging field of science that comprises the fabrication and characterization of nanomaterials for various applications such as medical, agricultural, and environmental pollution control [1]. At present, nanotechnology-based industries are growing rapidly, and deep investigation into this nanomaterial's health and environmental effects is highly needed [2]. Generally, organic and inorganic nanoparticles are produced in the industry. Organic nanoparticles are carbon and inorganic nanoparticles, including metal, silver, gold, magnetic, titanium dioxide, copper oxide, zinc oxide, and sulfide. Among inorganic nanoparticles, titanium dioxide nanoparticles ($TiO_2$NP's) are preferably used in the preparation of cosmetics, sunscreen lotions, and as a photocatalyst. $TiO_2$ is an important, highly stable material in aqueous solutions that is resistant to acidic and alkaline media; it is also easily recyclable, inexpensive, and non-toxic compared to other metals. It has been reported that the photocatalytic characteristics of $TiO_2$ are gained from the development of photo-generated charge carriers (holes and electrons) that are produced by UV light absorption [3].

Environmental pollution is considered one of the major concerns in general, and water pollution is prevalent all over the world. Textile, paper, and other industries are consuming various types of synthetic organic toxic dyes that are being directly released in large amounts into water bodies without proper treatment every day. The discharge of such toxic dyes into water bodies and soil environments affects water quality. It has also been found to act as a powerful mutagenic agent, eventually causing cancer and other disorders in aquatic organisms, animals, and humans [4]. In textile industries, various types of color dyes are being routinely utilized by 10–15% for producing colored fabrics. About 7–$10^5$ tons of dye substances are being released into the environment from textile industries alone. Almost 10,000 different colors of dyes are presently available for commercial applications. It is reported that most color dyes are highly toxic and carcinogenic to humans and animals and are also responsible for causing kidney problems, liver damage, and cancer [5]. It has been identified that the highly toxic property of crystal violet dye can cause not only cancer but also methemoglobinemia, inflammatory response in the gastrointestinal tract, cytogenetic toxicity, eye irritation, etc. The degradation of toxic organic dyes has been achieved using different techniques such as flocculation, electrocoagulation, UV-light degradation, and activated carbon [6]. Though various methods, such as adsorption, ion exchange, flocculation, etc., have been used to decrease the hazardous impact of dyes in the recent past, these procedures could not effectively remove or degrade the dye completely, and it caused additional pollution to the environment [7]. Among various methods used for dye removal, the nanotechnology-based photocatalytic dye degradation method under solar irradiation is considered the best way to remove the existing dye pollutant residues in the environment, including soil and water bodies. As a result, there is an urgent need to implement novel methods for reducing the toxic effects of textile dyes through degradation using nanocatalysts synthesized using a green chemistry approach.

Green chemistry-based nanotechnology has been widely adopted over physical and chemical methods due to its eco-friendly approach, synthesis on a large scale, and low cost [8]. With the help of stabilizing or capping bioactive molecules, the possibility of extracellular production of nanomaterials using an aqueous medium has been widely adopted in the recent past [9]. $TiO_2$NP's show an effective role in photocatalytic activity to effectively remove pollutants from contaminated environments due to the efficient degradation of organic dyes and phenol. It has been reported that the $TiO_2$NP's showed enhanced photocatalytic activity

due to their thermodynamic stability, relative non-toxicity, and strong oxidizing power. Green chemistry-based nanotechnology is identified as an alternative way to decrease the textile color dyes by using metallic NPs exposure through the mechanism of photocatalytic degradation by using solar irradiation; because these non-degradable dyes are released from textile industries that pollute the soil, water sources, and environment globally. Recently, plant-medicated *in vitro* synthesis of various nanoparticles, including $TiO_2$NP's has several advantages over other biological methods, and it is a rapid method for extracellular synthesis of nanoparticles on a large scale [10].

The potential antimicrobial activities of various metallic nanomaterials synthesized using different plant extracts via green chemistry methods have been described earlier. However, the conjugation of nanodrugs with antibiotics such as chloramphenicol, kanamycin, ampicillin, and erythromycin to AgNPs has also shown increased antimicrobial activity [11]. A biofilm is a form of a sticky gel consisting of polysaccharides, proteins, and other organic components on a wet surface area as well as in different clinical, industrial, and food processing environments. In addition, biofilm development in drinking water may lead to severe health and economic problems [12]. Nowadays, Pseudomonas aeruginosa is considered one of the most common nosocomial infections causing life-threatening agents. It causes various types of acute and chronic infections such as cystic fibrosis, burns, and urinary tract infections in humans. Also, it is difficult to either control or eradicates due to its high incidence of resistance to antimicrobial agents and biofilm formation. Further, various human pathogenic microorganisms have already developed resistance to commercially available antibiotic drugs that are commonly recommended to treat the infectious diseases causing methicillin-resistant *Staphylococcus epidermidis* (MRSE) and methicillin-resistant *Staphylococcus aureus* (MRSA).

Nanoparticles will react in an excellent way to degrade such biofilms and can inhibit further biofilm formation. Various plant extracts, including *Alternanthera sessilis*, are being used as capping and reducing agents for the biological synthesis of nanoparticles and are mostly used for environmental, biomedical, and pharmaceutical applications [13]. The anti-biofilm effect of metallic nanoparticles synthesized using plant extracts has been reported against biofouling bacterial strains such as *P. aeruginosa* and *S. epidermidis* demonstrating the antibiofilm activity of silver nanoparticles against *E. coli* and *K. pneumonia*. Prasannaraj and Venkatachalam described the efficient anti-biofilm activity of AgNP's engineered using various medicinal plant species, viz., *Centella asiatica*, *Plumbago zeylanica*, and *Semecarpus anacardium*. Earlier, Firdhouse and Lalitha [14-15] described the cost-effective biosynthesis of AgNP's using *Alternanthera sessilis* plant extracts and reported the enhanced cytotoxic activity against prostate cancer cells (PC3) by MTT assay. Ittiyavirah and Hameed reported the green synthesis of AgNP's using the ethanolic extract of *A. sessilis* (Linn.) and evaluated its anti-parkinsonian activity using an oxidative stress model of Parkinsonism using Rotenone. Recently, gold nanoparticles were synthesized using *Alternanthera philoxeroides*, and their antimicrobial activity was studied by Bhattacherjee [16]. *Alternanthera bettzickiana* plant extract was used to fabricate gold nanoparticles. The synthesized AuNPs exhibited efficient antibacterial activity against *Bacillus ubtilis, Enterobacter aerogenes, Micrococcus luteus, Pseudomonas aeruginosa, Staphylococcus aureus,* and *Salmonella typhi*. Also, the biosynthesized gold nanoparticles were tested to assess the cytotoxicity against A549 human lung cancer cell lines, and the results confirmed the efficient anticancer activity of the AuNPs [17]. Despite a few reports demonstrating the synthesis of nanoparticles and their antimicrobial

growth-inhibiting effects, studies pertaining to *A. sessils* leaf extract mediated synthesis of titanium nanoparticles, and their photocatalytic and biomedical applications are scanty. Therefore, the major focus of the present investigation was to bio-fabricate metallonanotitania catalysts using *Alternanthera sessilis* plants, which are available in large quantities and yet to be studied towards photocatalytic potential towards toxic textile dyes.

In this study, we mainly focused on rapid green engineering and characterization of biomolecule-wrapped AS@$TiO_2$NP's using aqueous leaf extracts of *A. sessilis*. The synthesized AS@$TiO_2$NP's were assessed for antibacterial activity and antibiofilm against perilous. The dye degradation was addressed against methylene blue and methyl orange. The stability and biocompatibility of AS@TiO2NP's detailed. The cytotoxicity of AS@$TiO_2$NP's was tested on non-cancerous and cancerous triple negative cancer cell lines.

## 2. Materials and Methods

### *2.1. Chemicals and bacterial strains.*

All the chemicals used in this study were of analytical grade. All lyophilized bacterial strains were procured from Microbial Typing Culture Collection (MTCC), Chandigarh, India, and American Tissue Culture Collection (ATCC). *Escherichia coli*-1610, *Pseudomonas aeruginosa*-1688, *Staphylococcus aureus*-96, and *Bacillus cereus*-430 strains were cultured in recommended broth as per the revival procedure provided by MTCC and ATCC. All the cell lines were procured from ATCC

#### 2.1.1. preparation of aqueous leaf extract.

In our previous study Sowmya *et al.* [18], a collection of plant and tissue culture techniques was represented in our previous study. Five grams of freshly generated *A. sessilis* plant tissues were placed in a 250 mL glass beaker containing 100 mL of MilliQ water. The beaker was microwaved for 2 min (LG microwave, 800 W) for 5 mins. After cooling, the extract was filtered through a Whatman filter No. 1 and a 0.22 µm nitrocellulose filter syringe to remove impurities. The extract was stored at 8$^{o}$ C until further processing.

### *2.2.Green synthesis of AS@$TiO_2$NP's by using tissue cultured A.sessilis leaf extracts.*

For fabrication of AS@$TiO_2$NP's, about 25 mL of filtered aqueous leaf extract was thoroughly mixed with 5 mM of 225 mL of $TiO_2$ solution. The reaction mixture was placed under light irradiation at room temperature for 24 h while the control setup was also kept without leaf extract. The occurrence of a color change indicates the formation of AS@$TiO_2$NP's. The reaction mixture was centrifuged at 8000 rpm for 10 min at room temperature. After carefully removing the supernatant, the nano pellets were collected and dissolved with MilliQ water. The dissolved AS@$TiO_2$NP's were washed thoroughly with MilliQ water, and the purified nanoparticles were kept for drying at 42°C. The dried nanoparticle powder was further utilized for characterization [19].

#### 2.2.1 UV-Vis spectroscopy.

The formation of AS@$TiO_2$NP's was assessed frequently by using a UV-visible double-beam spectrophotometer (UV-1800, Shimadzu, Japan) at the wavelength of 300-700nm to observe the surface plasmon resonance (SRP).

2.2.2. Dynamic light scattering (DLS) and Zeta size measurements analysis.

The synthesized AS@$TiO_2$NP's size distribution and stability were observed in accordance with Prasad *et al.* [20] with a Microtrac particle size analyzer (Montgomeryville, USA). The autoanalyzer provides a size distribution pattern of AS@$TiO_2$NP's.

2.2.3. Fourier transform infrared spectroscopy (FT-IR) analysis.

Further, the AS@$TiO_2$NP's nanoparticles were analyzed by Fourier transform infrared spectroscopy (FT-IR) for the presence of possible functional groups involved in the formation of nanoparticles (FT-IR Perkin-Elmer model spectrum RXI). Finally, the dried nanoparticle powder was compressed into a thin KBr disc within the range of 4000 to 400 $cm^{-1}$ in transmittance mode.

2.2.4. Scanning electron microscopic (SEM) and energy dispersive spectroscopic (EDX) analysis.

To elucidate the morphological structure of the synthesized AS@$TiO_2$NP's, one drop of diluted AS@$TiO_2$NP's was placed on a carbon-coated copper plate to air dry in-vacuum. The scanning electron microscopic analysis (SEM, HITACHI (S-3400N, Japan)) was performed with 10k voltage, and EDX analysis was used to confirm the presence of Ti ion on AS@$TiO_2$NPs with the HITACHI (Noran System 7, Oklahoma City, USA) system attached to SEM [21].

2.2.5. X-ray diffraction analysis.

The crystalline nature of AS@$TiO_2$NP's stability and particle size distribution were also characterized by X-Ray diffraction (XRD) experimental analysis. The XRD experiment was carried out on Rigakuminiflex II operated at a voltage of 40 kV, a current of 30 mA, and a scan rate of 10°C/min with Cu-Kα radiation in a θ–2θ. UV-visible spectral analysis [22].

*2.3. Colloidal stability.*

100 µg/mL of synthesised AS@$TiO_2$NP's were dissolved in millipore water, and the solution colloidal stability was assessed using UV-Vis spectroscopy at 390 nm over a period of time [23].

*2.4. Study on stability of AS@$TiO_2$NP's with respect to pH, salinity, and temperature.*

The stability of the synthesized AS@$TiO_2$NP's was studied by varying the ionic strength in the aqueous medium (NaCl) from 0.2 to 1 M at a balanced pH. In the same way, the consistency of AS@$TiO_2$NP's was monitored for temperature from 30-90$^oC$ and pH 2-10, respectively [24].

*2.5. Antibacterial activity of AS@$TiO_2$NP's by disc diffusion assay.*

To evaluate the antimicrobial potential of AS@$TiO_2$NPs, four human pathogenic bacteria were used, viz, *E. coli, S. aureus, P. aeruginosa,* and *B. cereus,*and antimicrobial efficacy was determined using the disc method on nutrient agar plates. The nutrient agar medium was sterilized by autoclaving at 121°C for 15 min. About 20 mL of sterilized medium was dispensed into each sterile Petri plate and kept inside the laminar airflow hood for

solidification of the medium. About 100 µL of overnight bacterial culture was aliquoted onto plates and was evenly spread using a glass spreader. Finally, the sterile discs (6 mm) were carefully placed on a nutrient agar medium by opening the Petri dishlid. 6 µL of different concentrations of AS@$TiO_2$NPs was dispensed to discs in the same way as plant extract was compared to standard antibiotic (streptomycin). Subsequently, the nutrient agar plates were placed inside the bacteriological incubator and maintained at 37°C for 12 h. The zone of bacterial cell growth inhibition rate was calculated by using a scale and expressed in mm [25].

*2.6. Bacterial cell damage by Scanning electron microscope (SEM).*

The *S. aureus* and *P. aeruginosa* cultures were used for cell membrane damage studies by treating them with double the minimum inhibitory concentration of AS@$TiO_2$NP'sfor 2 h. The treated culture was centrifuged at 1000 rpm for 5 min. Finally, cells were smeared on a glass slide with the help of 2.5% glutaraldehyde in a phosphate buffer solution. The deposited cells were treated with 30–100% ethanol stepwise to dry, and SEM images were taken after 2 days [26].

*2.7. Measurement of the influence of AS@$TiO_2$NP's on antibiofilm activity.*

The anti-biofilm activity of AS@$TiO_2$NP's was studied qualitatively and quantitatively by the method adopted [27]. Briefly, 100µL of *S.aureus* and *P. aeruginosa* cell culture was dispensed in a separate tissue culture plate containing 1800µL of BHI broth supplemented with glucose. To each well, dispense a different graded concentration of AS@$TiO_2$NP's and incubate at 37°C for 18 h. The biofilm-developed wells were washed thrice with sterile phosphate buffer solution, and cells were fixed by adding 250µL of methanol for 20 min, air dried, and stained with 0.5% crystal violet for 15 min. The wells were allowed to dry completely and washed thrice to remove the excess stain. Finally, 150 µL of 95% ethanol was added to elute the dye. The OD of the eluent was measured at 490 nm in a microtiter plate spectrophotometer. All assays were performed in triplicates.

*2.8. Catalytic degradation of methyl orange (MO) and methylene blue (MB).*

The dye degradation activity of AS@$TiO_2$NP's was evaluated to quantify the degradation effects of methyl orange and methylene blue dyes by using sodium borohydride as a catalyst to accelerate the reaction process [28]. 10mL of each dye (100 ppm) was dispensed in a separate glass tube containing 1 mL of $NaBH_4$ (1 g in 10 mL) and then treated with different concentrations of synthesized AS@$TiO_2$NP's. Every 5 minutes, the dye degradation was recorded at max 460 and 664 for MO and MB, respectively. The percentage of dye degradation was calculated by using the formula.

$$C\ (\%) = [A_0 - At]/\ A_0 \times 100$$

where A0 = Absorbance of untreated dye, At = Absorbance of treated dye with AS@$TiO_2$NP'sat different interval is time and C = percentage of dye degradation [29].

*2.9. Bio-compatibility.*

2.9.1. RBC's hemolysis rate.

The various concentrations of AS@$TiO_2$NP's(1.5, 3.1, 6.75, 12.5, 25, and 50 mg/kg) were dispensed to freshly drawn sheep blood, incubated at 37°C for 30 min and centrifuged at

3000 rpm for 5min. The absorbance of the supernatant was measured at 545 nm. The hemolysis rate (HR) was calculated using the below formula [30].

HR= OD treated − OD negative control / OD positive control – OD negative control x100.

Samples were considered highly hemocompatible if HR<5%, hemocompatible if HR<10%, and non-hemocompatible if HR > 20% [30].

*2.10. Cytotoxicity of AS@$TiO_2$NP's against normal and cancerous cell lines.*

2.10.1.Preparation of cell lines and culture medium.

All cell lines were obtained from the ATCC gene bank and sub-cultured in DMEM supplemented with 10% inactivated Fetal Bovine Serum (FBS), penicillin (100 IU/mL), and streptomycin (100 g/mL) at 37ºC in a humidified atmosphere of 5% $CO_2$. The cell was dissociated with a cell-dissociating solution (0.2 % trypsin, 0.02 % EDTA, 0.05 % glucose in PBS). The viability of the cells is checked and centrifuged. In addition, 50,000 cells were inoculated per well in a 96-well plate and incubated for 24 hours at 37ºC in a 5% $CO_2$ incubator [31].

2.10.2. MTT assay.

The monolayer cell culture was trypsinized, and the cell count was adjusted to 5 x $10^5$ cells/mL using a medium containing 10% FBS. To each well of the 96-well microtiter plate, 100µL of the diluted cell suspension (50,000 cells/well) was added. After 24 h, when a monolayer was formed, the supernatant was flicked off, the monolayer was washed once with medium, and 100µL of different test concentrations of test drugs were added to the monolayer in microtiter plates. The plates were then incubated for 24 hours at 37ºC in a 5% $CO_2$ atmosphere. After incubation, the test solutions in the wells were discarded, and 100 µL of MTT (5 mg/10mL of MTT in PBS) was added to each well. The plates were incubated for 4 h at 37°C in a 5% $CO_2$ atmosphere. After removing the supernatant and adding 100 µL of DMSO to dissolve the formed formazan, the plates were gently shaken. The absorbance was assessed using a microplate reader at a wavelength of 590 nm. The concentration of the test substance required to reduce cell growth by 50% and calculate the percentage growth inhibition was calculated using the formula below ($IC_{50}$ ). Values were generated from the dose-response curves for each cell line [32].

Inhibition is calculated as ((OD of Control - OD of Sample)/OD of Control) x 100.

*2.11. Statistical analysis*

For statistical analysis, each experiment was carried out with three replicates and repeated all the experiments at least thrice. All data obtained were statistically analyzed by applying ANOVA. Data were presented as the mean ± standard error (SE). The mean separations were carried out using Duncan's multiple range tests, and significance was determined at the *P*>0.05 % level [33].

## 3. Results and Discussion

### *3.1. Synthesis and characterization of AS@TiO$_2$NP's.*

The AS@TiO2NP's were synthesized by adding *Alternanthera sessilis* plant tissue extract as a reducing agent to 5 mM $TiO_2$. The formation of the AS@$TiO_2$NP's was confirmed by changing the white color suspension to a creamy yellow color. The UV- Vis spectral pattern established the color change of colloidal AS@TiO2NP's. The surface plasmon resonance (SPR) of AS@$TiO_2$NP's showed maximum absorption at 390 nm, and the stability of the NP's was confirmed even after one month (Figure 1). The color arises because of the excitation of surface plasmon resonance (SPR) of the $TiO_2$NPs. Sankar*et al*. reported similar color alterations during the synthesis of $TiO_2$NPs using *Azadirachta indica* leaf extracts [34].

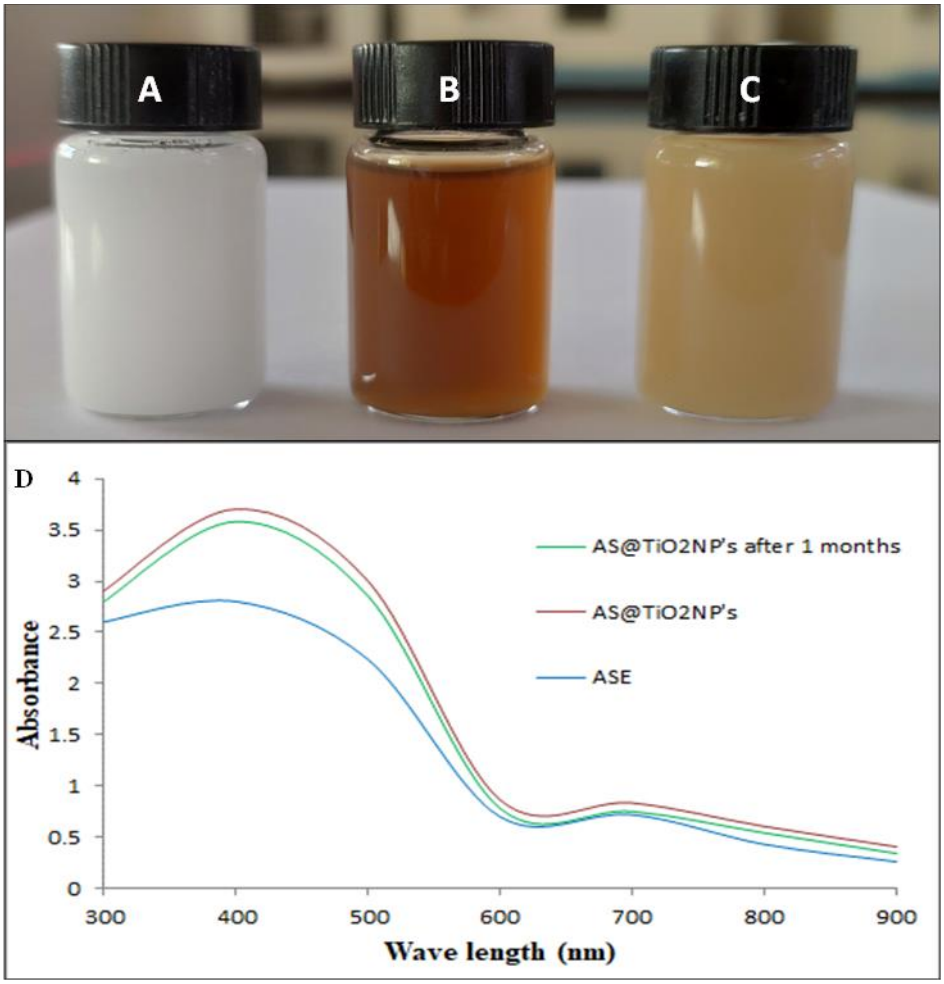


**Figure 1.** Biogenic synthesis and UV–Vis spectra of *A. sessilis* plant tissue titanium nanoparticles (AS@$TiO_2$NP's). (**A)** Aqueous 5 mM TiO2 solution, (**B)** *A. sessilis* plant tissues extract,**(C)**AS@$TiO_2$NP formation, and (**D)**The synthesized AS@$TiO_2$NP's was dissolved in MilliQ water, and spectral readings were recorded from 300 to 900 nm wavelength ranges, which also represent the stability of the nanoparticles even after one month.

The absorbance spectrum was extremely sensitive to the nature, size, and shape of the nanoparticles produced, their inter-particle distances, and the surrounding medium. Moreover, a variation in the biological material concentration is known to influence nanoparticle synthesis. Initially, the UV-visible spectroscopy analysis was performed to measure the reduction of titanium ions in the reaction solution. It is well known that the optical absorption spectrum of metal nanomaterials is dominated by the surface plasmon resonance that shifts to

longer wavelengths with increasing nanoparticle size due to the interaction of capping agents present in the leaf extract[35]. Generally, the number of SPR peaks decreases as the symmetry of the nanoparticles increases. In the present study, the $TiO_2$ NPs formation was confirmed by a spectrum at 390 nm. Metallic titania nanoparticles can be synthesized by reducing metal ions with some chemical molecules, whereas in photosynthesis, plant material extracts containing biological macromolecules are thought to act as a reducing agent for the development of nanoparticles in the reaction mixture. Umar and Cumbal also recorded an absorption peak at 350 nm for the synthesis of $TiO_2$ NPs nanoparticles using *Citrus paradsi* peel extract. Ganesan *et al*. observed the UV spectrum at 332 nm for producing nanotitania catalysts using *A. altissima* leaf extracts[36]. The Fourier transform infrared spectroscopy (FT-IR) analysis was performed to identify the possible functional groups that are involved in the bio-reduction of titania nanoparticles. The general observation of the FT-IR data confirms some bioactive compounds bound to the surface of bioengineered AS@$TiO_2$NP's that could be responsible for the bio-reduction, capping, and stabilization of nanomaterials (e.g., phenolic compounds, organosulfur compounds, amino acids, and carbohydrates).

FT-IR data exhibited the potential functional groups available in the leaf extracts of *Alternanthera sessilis* that are believed to be responsible for forming AS@$TiO_2$NP's (Figure 2). The FT-IR spectrum shows the absorption peak at 3435.89 $cm^{-1}$ corresponding to O-H bending, which indicates the presence of alcohol and phenol groups. The spectra at 1643.69.83 $cm^{-1}$ correspond to a C-O stretch, indicating the occurrence of ether and alcohol groups, respectively. Other absorption peaks at 1033.90 $cm^{-1}$ (C-N stretch), 691.76 $cm^{-1}$ (C-H stretch), and 1643.69 $cm^{-1}$ (C-C stretch) may indicate the possible presence of aliphatic amines, aromatic and C=C, respectively. It is believed that these bioactive compounds might have been involved in the bio-reduction of AS@$TiO_2$NP's. Santhosh Kumar *et al*. [37] also reported similar functional groups from *Psidium guajava* plant extract. Earlier studies show that the phenolic molecules, carboxylic acids, amines, and amides from different plant extracts are responsible for the bioreduction process, while the stability of AS@$TiO_2$NP's might be due to the presence of free amino and carboxylic groups. The particle size, shape, and distribution of colloidal particles of AS@$TiO_2$NP's were assessed by DLS and SEM, which indicated the AS@$TiO_2$NP's average 69 nm with 6.5 mV by DLS. The SEM image analysis confirmed the surface and morphology of the synthesized AS@$TiO_2$NP's and found them to be crystalline in shape (Figure 3A & B).

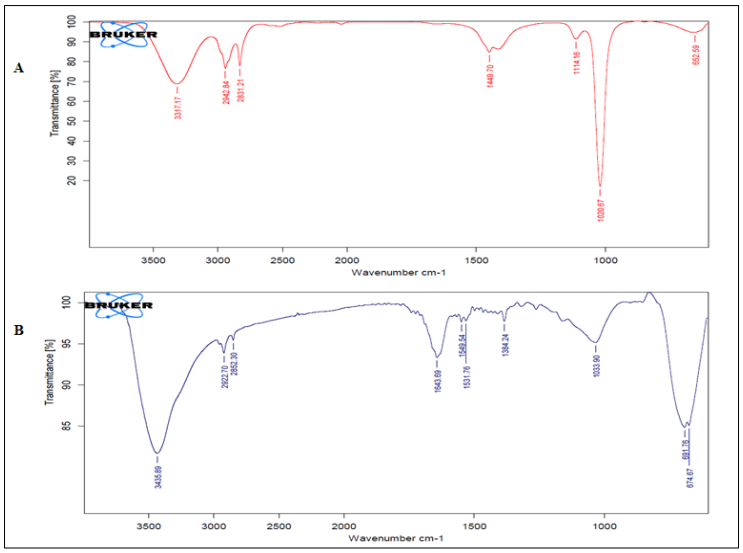


**Figure 2.**FT-IR spectra of AS@$TiO_2$NP's. (**A)** Indicate the plant extract and (**B)** AS@$TiO_2$NP's.

The XRD analysis of AS@$TiO_2$NP's displays several size-dependent features, leading to an irregular peak position, height, and width. The XRD result confirms the crystalline nature of the green synthesized AS@$TiO_2$NP's. Diffraction peaks were linked to the 2θ values of 25.17°, 37.73°, 47.91°, 53.83°, 54.96°, 62.71°, and 75.2°, which correspond to the (101), (004), (200), (105), (211), (118) and (215) planes of the standard cubic phase of titanium. The existence of diffraction peaks matched the standard data files (JCPDS card no: 21-1272) for all reflections (Figure 4). Similarly, XRD analysis of $TiO_2$ nanoparticles exhibited a crystalline nature with the same 2θ value at 25.32 anatase form of 101 rutile using the green synthesis method [38].

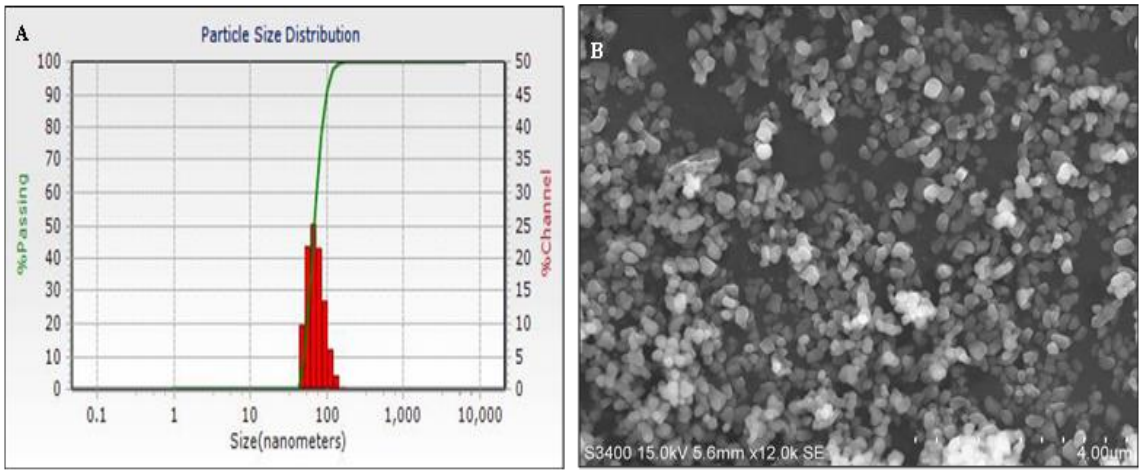


**Figure 3. (A)** The size distribution of synthesized AS@$TiO_2$NP's, **(B)** Scanning electron microscope image of spherical AS@$TiO_2$NP's.

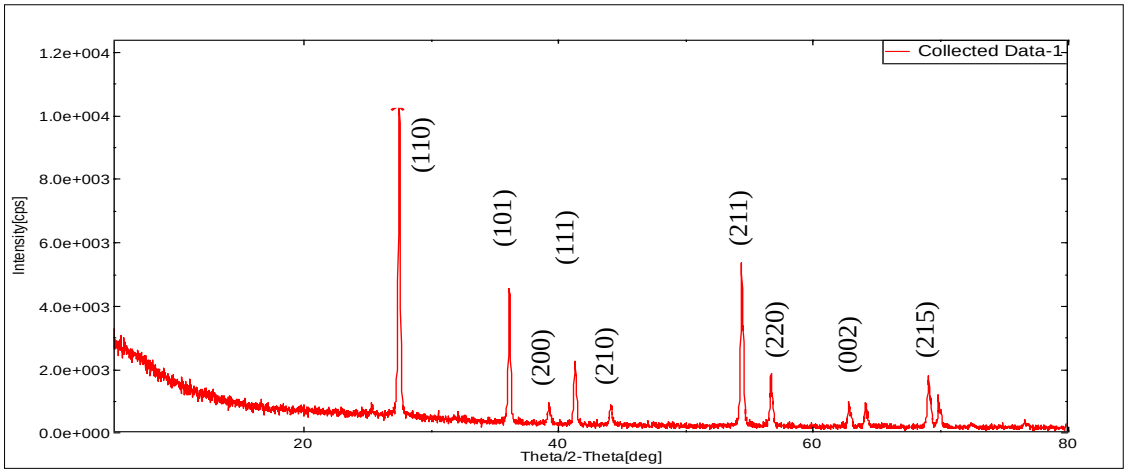


**Figure 4.** XRD analysis of AS@$TiO_2$NP's diffraction peaks were linked to the 2θ values of 25.17°, 37.73°, 47.91°, 53.83°, 54.96°, 62.71°, and 75.2° which corresponds to the (101), (112), (200), (105), (211), (116) and (215) planes of the standard cubic phase of titanium.

Energy dispersive X-ray (EDX) analysis exhibits a strong peak which confirms the presence of titanium ions in the synthesized nanoparticles (Figure 5). The present results are in agreement with an earlier report on the synthesis of titanium dioxide nanoparticles in different plant species, including *Mangifera indica* and *Azadirachta indica* plant extracts, *Parthenium hysterophorus*, and *Euphorbia hirta* [39].

*3.2.The colloidal stability of AS@$TiO_2$NP's in induced pH, temperature and salanity.*

Different pH ranges from 2 to 10 were used to study the impact of pH on AS@$TiO_2$NP's stability. As per the data, AS@$TiO_2$NP's was most stable at a pH of 8, as shown by the

absorbance at 390 nm (Figure 6A). By dissolving AS@$TiO_2$NP's in PBS with 0.2-1 M NaCl, the ionic strength of the material was assessed, and absorbance was assessed using UV-Vis spectra. A distinctive peak for AS@$TiO_2$NP's is located at 390 nm. The data showed that AS@$TiO_2$NP's was stable up to 0.4 M and that, above this concentration, the peak was broadened (Figure 6B). Finally, the effect of temperature at 30 and 90 °C was investigated. In the 30 –70 °C range, AS@$TiO_2$NP's remained stable (Figure 6C).

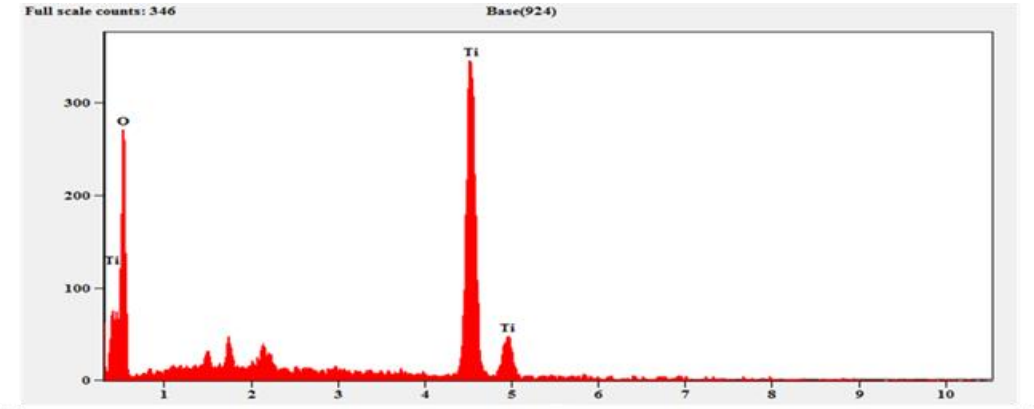


| Element Line | Weight % | Weight % Error | Atom % |
|---|---|---|---|
| O K | 40.05S | --- | 66.67 |
| Ti K | 59.95 | ± 1.18 | 33.33 |
| Ti L | --- | --- | --- |
| Total | 100.00 | | 100.00 |

**Figure 5.** Energy dispersive X- ray (EDX) analysis of AS@$TiO_2$NP's.

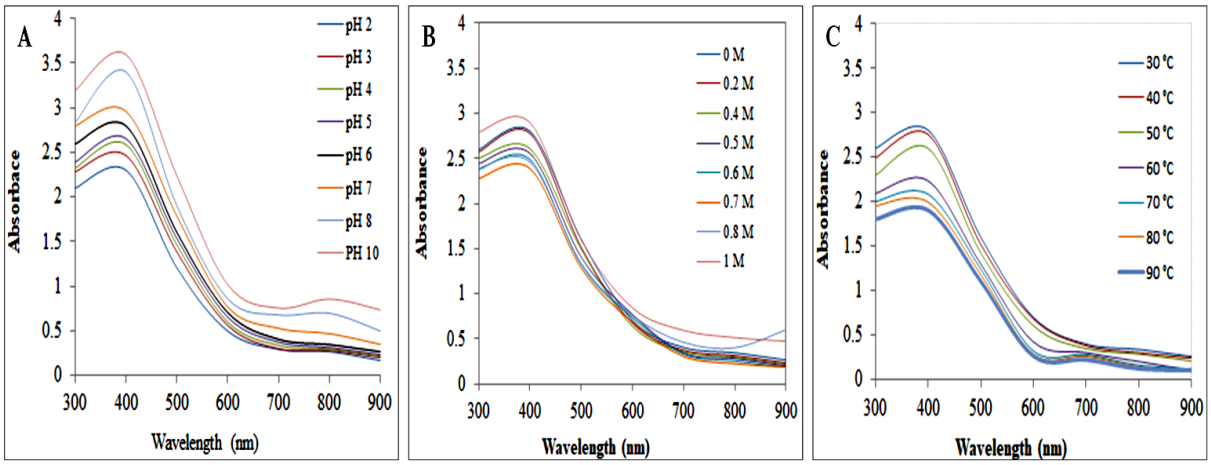


**Figure 6.** Stability of AS@$TiO_2$NP's with respect to (**A**) pH, (**B**) temperature, and (**C**) salinity.

*3.3. Antibacterial activity of AS@$TiO_2$NP's.*

The antimicrobial efficacy of the AS@$TiO_2$NP's was examined using the extended-spectrum β-lactamase (ESBL) producing Gram-negative *P.aeruginosa*, and *E.coli*, Gram-positive methicillin-resistant *S. aureus* (MRSA), and *B. cereus* bacterial strains by growth inhibition test (Figure7). The results of the antimicrobial effects of AS@$TiO_2$NP's exposure are depicted in Table 1. Results of this investigation clearly showed the zone of bacterial cell growth inhibition around each disc placed on agar plates treated with AS@$TiO_2$NP's, leaf extract, and antibiotics (Figure 7A, B, C & D). The highest rate of growth inhibition recorded was 27.42 mm to *E.coli* at 100 µg/mL of $TiO_2$NPs dose, followed by *P. aeruginosa* (24.40 mm), *S. aureus* (23.80 mm) and *B. cereus* (17.80)(Figures 7C, D, E & F). The present results strongly suggest that gram-negative bacterial strains were found to be more susceptible to the

exposure of AS@$TiO_2$NP's than gram-positive bacterial strains. It is assumed that the occurrence of various bioactive compounds in the leaf extracts might be one of the reasons that they could be slowly released from AS@$TiO_2$NP's during the exposure in a sustainable manner on the bacterial cell surface and may induce apoptosis by inhibiting the bacterial cell respiration mechanism and permeability. Thei's a possible mode of action could be related to its attachment with bioactive molecules of the thiol group found in the respiratory enzymes of pathogens.

Furthermore, Ti ion interrelation with the bacterial cell membrane may influence the cell respiratory enzyme level by degrading DNA or proteins, which could eventually suppress the bacterial cell's growth. Present observations are in agreement with earlier reports, including Sundrarajan *et al*. [40], who reported an efficient anti-bactericidal efficacy of titanium dioxide nanoparticles with pathogenic bacterial isolates. Similarly, Keerthika *et al.* [41] also reported that AS@$TiO_2$NP's catalysts exhibited remarkable antimicrobial effects against both gram-positive as well as gram-negative bacterial pathogens. It has been reported that the cell wall of gram-positive bacterial strains has a thick and rigid peptidoglycan layer and lipoteichoic acids that have a strong negative charge. This might be considered one of the possible reasons for showing lower antibacterial activity with gram-positive bacterial strains than with gram-negative bacteria.

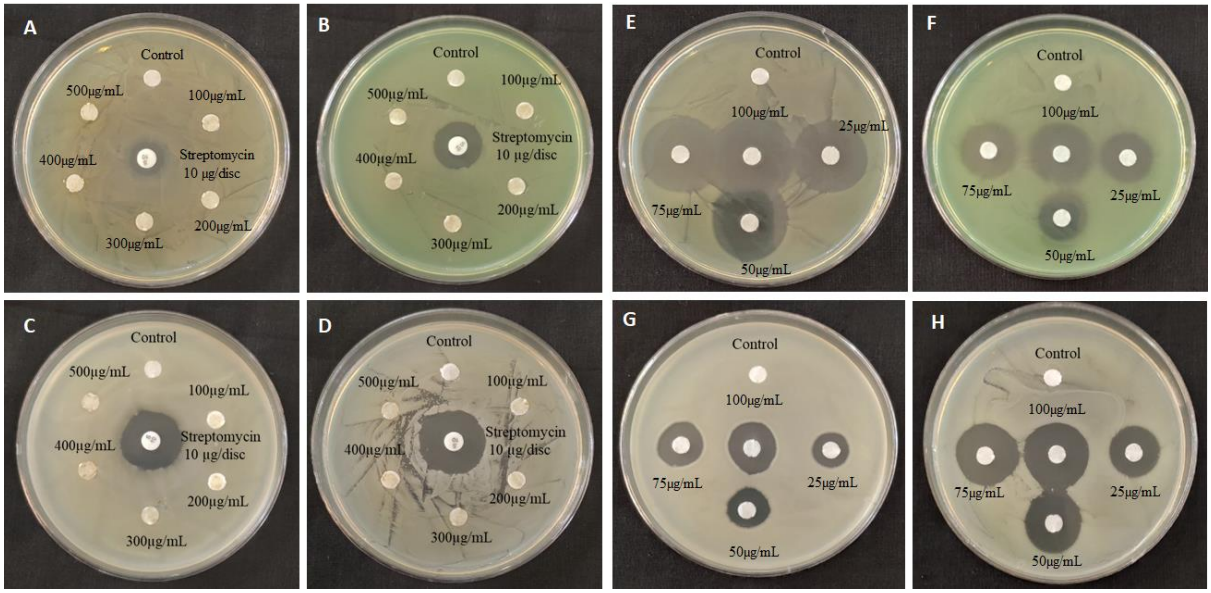


**Figure 7.** Antibacterial activity of AS@$TiO_2$NP's against perilous pathogenic bacteria. The disc diffusion assay was done to measure the MIC values of AS@$TiO_2$NP's against disease-causing pathogens. **A, B, C,** and **D:** Images depict *A. sessilis* plant tissues extracted at different concentrations against *E. coli, P. aeruginosa, B. cereus,* and *S. aureus,* respectively, in comparison to streptomycin drug (10 µg/disc). **E, F, G, and H:** Images represent the AS@$TiO_2$NP'sin various concentrations against *E. coli, P. aeruginosa, B. cereus,* and *S. aureus,* respectively.

*3.4. Bacterial cell damage study.*

The scanning electron microscopic images of the bacterial cell damage of *S. aureus* and *P.aeruginosa* cells treated with AS@$TiO_2$NP's are presented in Figure 8. In the untreated sample, the surface of bacterial cells was smooth and showed typical characteristics of the surface of native cells, such as smooth and intact, while cells treated with NPs appeared severely damaged. Some cells showed large leakage, while others were misshapen with many pits and gaps in their membrane [42].

**Table 1.** Antibacterial activity of *A. sessilis* plant tissues and AS@$TiO_2$NP's against perilous pathogens.

| **Test Microorganisms** | **AS@$TiO_2$NP's (Zone of inhibition in mm)** | | | | | |
|---|---|---|---|---|---|---|
| | **25 µg/mL** | **50 µg/mL** | **75 µg/mL** | **100 µg/mL** | **Streptomycin 10µg** | **Negative control** |
| **Gram-positive** | | | | | | |
| *Staphylococcus aureus* | 16.40±0.04$^{b}$ | 18.60±0.06$^{b}$ | 20.62±0.08$^{b}$ | 23.80±0.03$^{c}$ | 22.60±0.08$^{a}$ | NI |
| *Bacillus cereus* | 9.40±0.01$^{d}$ | 10.20±0.02$^{d}$ | 12.60±0.01$^{d}$ | 17.80±0.02$^{d}$ | 20.30±0.08$^{b}$ | NI |
| **Gram-negative** | | | | | | |
| *Escherischia coli* | 18.82±0.05$^{a}$ | 22.10±0.04$^{a}$ | 24.12±0.06$^{a}$ | 27.42±0.07$^{a}$ | 12.80±0.04$^{d}$ | NI |
| *Psuedomonas aeruginosa* | 14.64±0.04$^{c}$ | 16.80±0.05$^{c}$ | 19.20±0.06$^{c}$ | 24.40±0.08$^{b}$ | 16.40±0.06$^{c}$ | NI |
| **Test Microorganisms** | ***A. sessilis* plant tissues extract (Zone of inhibition in mm)** | | | | | |
| | **250 µg/mL** | **500 µg/mL** | **750 µg/mL** | **1000 µg/mL** | **Streptomycin 10µg** | **Negative control** |
| **Gram-positive** | | | | | | |
| *Staphylococcus aureus* | NI | NI | NI | NI | 22.60±0.08$^{a}$ | NI |
| *Bacillus cereus* | NI | NI | NI | NI | 20.30±0.08$^{b}$ | NI |
| **Gram-negative** | | | | | | |
| *Escherichia coli* | NI | NI | NI | NI | 12.80±0.04$^{d}$ | NI |
| *Pseudomonas aeruginosa* | NI | NI | NI | NI | 16.40±0.06$^{c}$ | NI |

Values are means of three independent replicates(n=1) ± indicate standard errors. Means followed by the same letter(s) within the same column are not significantly ($P \leq 0.05$) difference according to Turkey'sHSD.

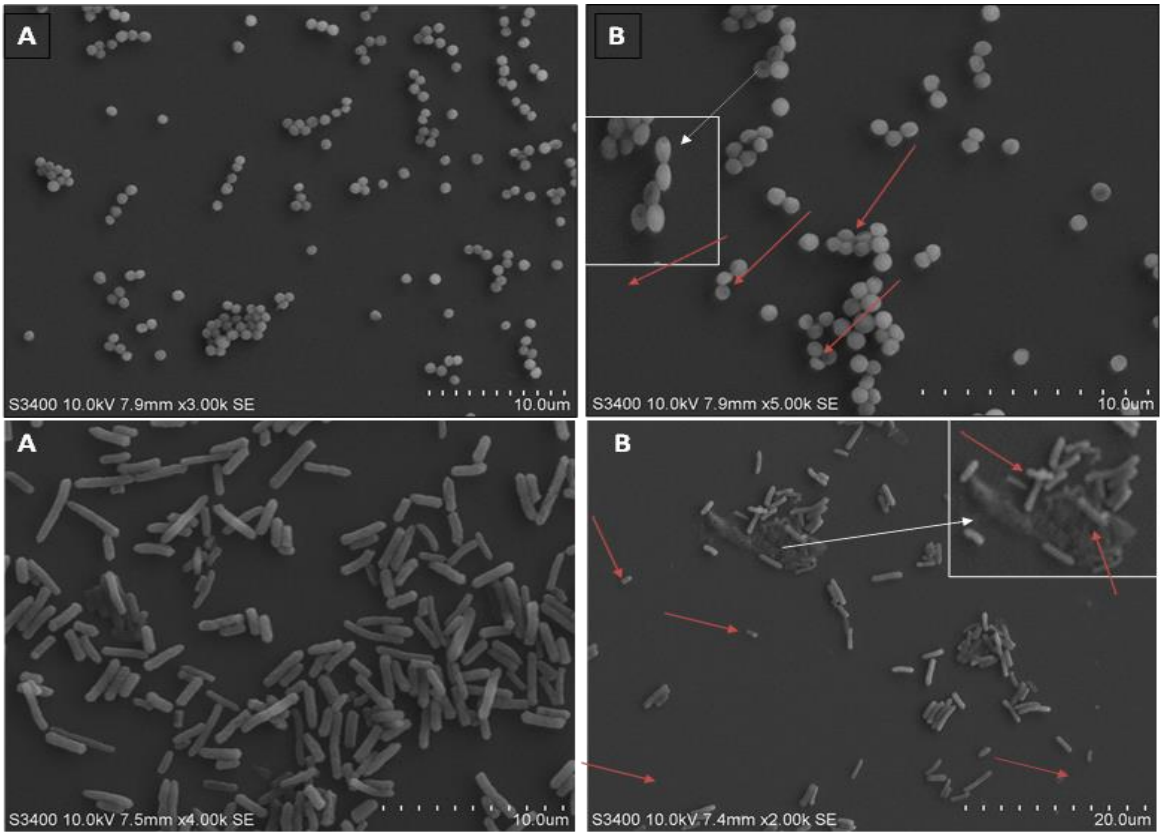


**Figure 8.** The cell membrane damage was shown in the SEM images. Compared to that of control, *S. aureus* and *P. aeruginosa*, after incubating with AS@$TiO_2$NP's for 2 h, showed changes in their respective membranes (A and B) (without treatment). Arrow marks demonstrated the membrane change.

*3.4. Effect of AS@$TiO_2$NP's on antibiofilm activity.*

Biofilm is considered a protective coat of aggregated bacterial cells associated with the substratum and consists of extracellular polysaccharides (EPS) that could play an important role during pathogenesis and is also responsible for extending various infectious diseases, particularly at the time of medical implant treatments. Both *P. aeruginosa* and *S. aureus* bacterial strains might exhibit acute resistance by developing biofilm coats and becoming resilient to host immune responses and antibiotics. Bacterial growth could be effectively controlled by antibiotic treatment. However, the possibility of individual pathogens may exist if the development of slime decreases virulence. This incidence may reinitiate the disease again even after completing the treatment. Therefore, it is a prerequisite to controlling biofilm formation by nanoparticle treatment, and it is considered a promising tool to resist the MDR bacterial strains. Therefore, the major focus of this investigation was to investigate the potential antibiofilm performance of biomolecules coated with AS@$TiO_2$NP's against gram-positive and gram-negative human pathogens. To assess the antibiofilm activity, various doses of biomolecules coated with AS@$TiO_2$NP's (250, 500, 750, and 1000 µg/mL) were tested against *P. aeruginosa* and *S. aureus*. The results of antibiofilm activity induced by AS@$TiO_2$NP's exposure are presented in Figure 8. The frequency of antibiofilm efficacy upon exposure toAS@$TiO_2$NP's catalysts ranged from 55.22, 43.07, 31.059, 22.29 % and 43.62, 15.32, 10.60, 6.87 % for *S. aureus* and *P. aeruginosa* respectively (Figure 9A & B). It is noteworthy to indicate that the formation of biofilm was decreased with increasing the concentration of AS@$TiO_2$NP's. Results suggest that AS@$TiO_2$NP's exposure showed potent inhibition of biofilm development by *S. aureus* as well as *P. aeruginosa* due to the slow and sustainable

release of biomolecules coated with Ti ions into the medium in a concentration-dependent manner.

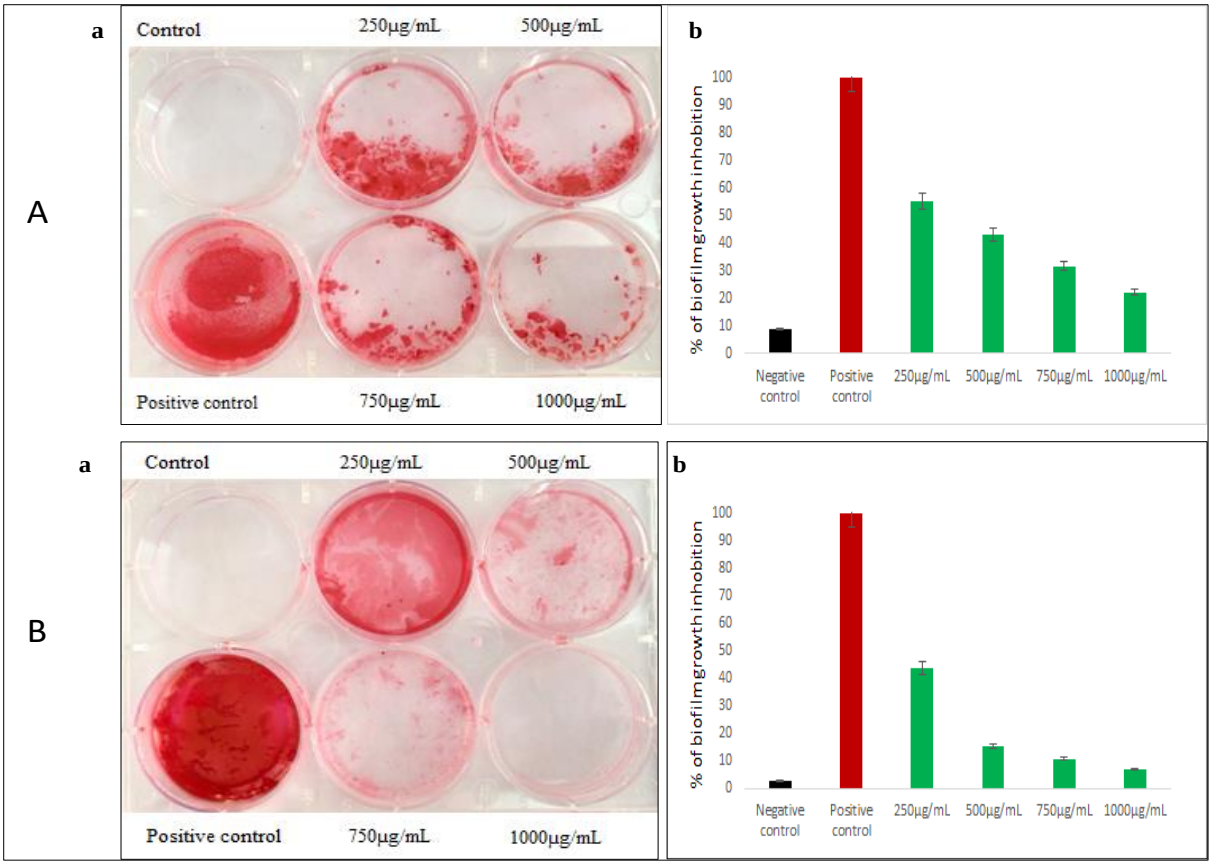


**Figure 9.** Antibiofilm activity of AS@$TiO_2$NP's against *S. aureus* and *P. aeruginosa*. (**A)** images Aa and Ab represent the qualitative and quantification of antibiofilm activity against *S. aureus*. (**B**) images Aa and Ab represent the qualitative and quantification of antibiofilm activity against *P.aeruginosa*.

The present observation was consistent with the safranin staining test, and the results strongly suggest that bioactive molecules coated with AS@$TiO_2$NP could play a pivotal role in the detected biofilm inhibition test. Due to the presence of water channels in the biofilm, metallic AS@$TiO_2$NP's can effectively transmit via the cell membrane exopolysaccharide layer, eventually inhibiting bacterial cell growth. Similarly, a significant reduction of biofilm-forming ability was observed in the presence of titanium dioxide nanoparticles, suggesting a decreased level of EPS production. The present results strongly suggest that biomolecule-coated AS@$TiO_2$NP's serve as potential nanodrugs for bacterial cell growth inactivation and interruption of biofilm development.

### *3.5. Dye degradation activity of AS@$TiO_2$NP's.*

The revealed data suggests that the toxic dye was gradually degraded due to the presence of AS@$TiO_2$NP's. It is assumed that the occurrence of high frequencies of dye degradation was due to the presence of various bioactive compounds on the surface of the AS@$TiO_2$NP's. Further, this result confirms that the AS@$TiO_2$NP's can effectively degrade the toxic organic pollutants within 15 min, and that these AS@$TiO_2$NP's were found to be highly stable for dye degrader applications (Figures 10 & 11) &Table 2. It is noteworthy that the bio-fabricated AS@$TiO_2$NP's acted as an efficient anionic and cationic degradation of toxic organic dyes because of their strong oxidizing power, non-toxicity, and long-term stability.

Current results strongly suggest that AS@$TiO_2$NP's can be applied to remove toxic dyes in contaminated environments due to their low cost and high photostability properties. Moreover, the green-engineered AS@$TiO_2$NP's can be used as a promising nanocatalyst for the potential degradation of toxic organic dyes that are non-biodegradable. Similarly, AS@$TiO_2$NP's was successfully used for the effective activity of industrially important organic toxic dyes synthesized using extracts of *Parthenium hysterophorus* and *Euphorbia hirta*.

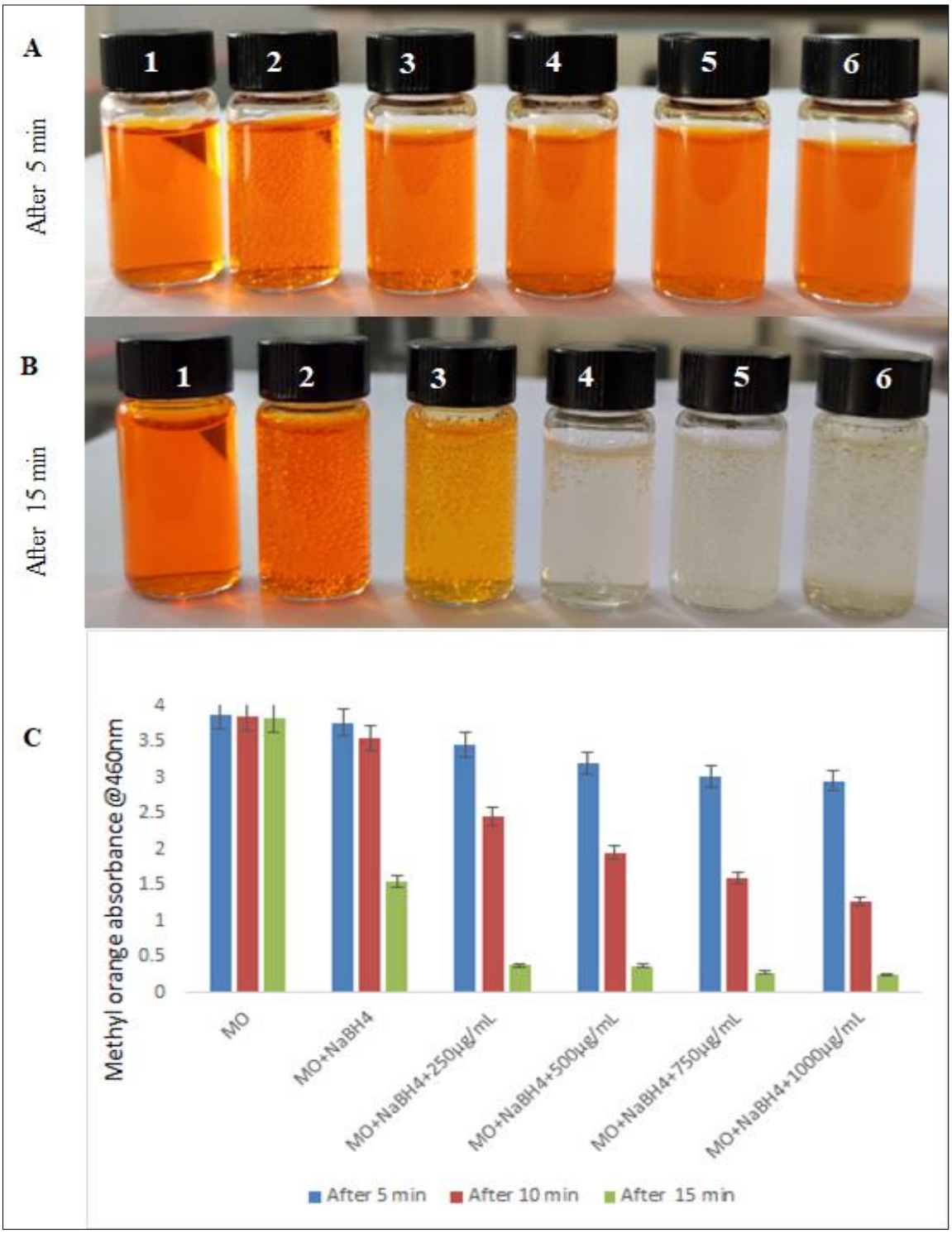


**Figure 10.** Dye degradation study of methyl orange (MO). (**A)** and (**B)** Represent the color imagining of MB dye degradation after treatment with AS@$TiO_2$NP's at 5 and 15 min intervals.

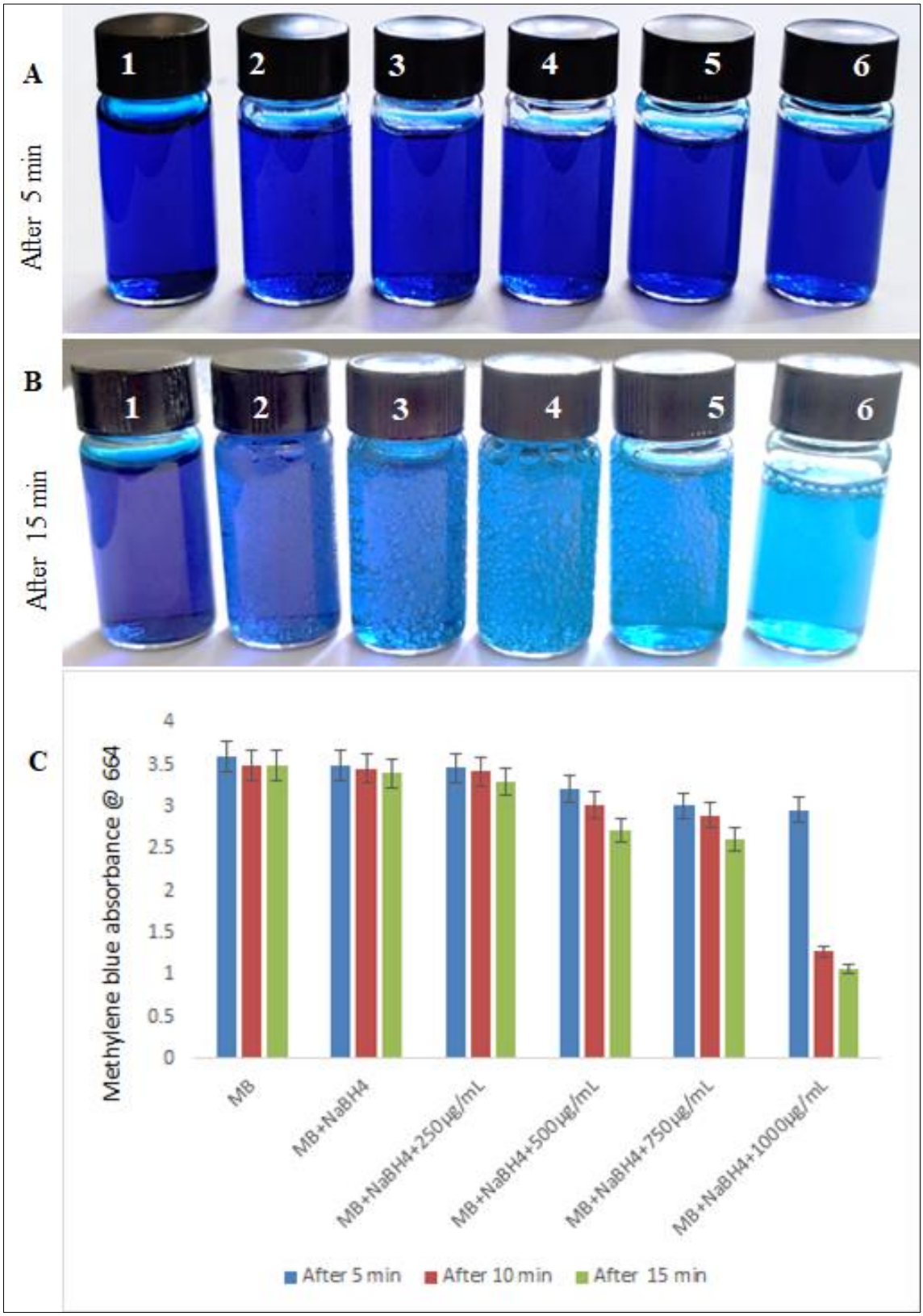


**Figure 11.** Dye degradation study of methylene blue (MB). (**A)** and (**B)** Represent the color imagining of MB dye degradation after treatment with AS@$TiO_2$NP's at 5 and 15 min intervals.

**Table 2**. % of dye degradation of MO and MB in the presence of $NaBH_4$ catalyst and different concentrations of AS@$TiO_2$NP's.

| Volume used (mL) | Amount of $NaBH_4$ added (µg) | Amount of AS@$TiO_2$NP's added(µg) | Dye degradation (%) | | |
|---|---|---|---|---|---|
| | | | After 5 min | After 10 min | After 15 min |
| Methyl orange (MO) | | | | | |
| 10.0 | 0.0 | 0.0 | 0 | 0 | 0 |
| 10.0 | 100.0 | 0.0 | 3.43 | 8.71 | 60.00 |
| 10.0 | 100.0 | 250 | 11.28 | 36.92 | 90.07 |
| 10.0 | 100.0 | 500 | 17.84 | 49.74 | 90.28 |
| 10.0 | 100.0 | 750 | 22.66 | 58.92 | 92.66 |
| 10.0 | 100.0 | 1000 | 24.10 | 67.18 | 93.66 |
| Methylene blue (MB) | | | | | |
| 10.0 | 0.0 | 0.0 | 0 | 0 | 0 |
| 10.0 | 100.0 | 0.0 | 3.32 | 4.43 | 5.61 |
| 10.0 | 100.0 | 250 | 3.88 | 5.26 | 8.53 |
| 10.0 | 100.0 | 500 | 11.25 | 16.34 | 24.76 |
| 10.0 | 100.0 | 750 | 16.45 | 19.66 | 27.67 |
| 10.0 | 100.0 | 1000 | 18.00 | 64.54 | 70.58 |

*3.6. Biocompatibility nature of AS@$TiO_2$NP's at hemostatic condition.*

Erythrocytes are maintained in good osmotic condition inside the bloodstream. RBCs immediately go through hemolysis and release hemoglobin as a condition of an unbalanced osmotic pressure and physical change. After being treated with AS@$TiO_2$NP's, it revealed no alterations in the membrane. The colorimetric approach was used to calculate the hemolysis rate.The impact of AS@$TiO_2$NP's on erythrocytes was assessed, and the results showed that they were biocompatible with no significant hemolysis (5%) at concentrations ranging from 1.5, 3.1, 6.25, 12.5, and 25 mg/Kg. RBCs significantly changed after the concentration was increased to 50 mg/Kg, and hemolysis (6.2%) was evidenced (Figure 12A & B).

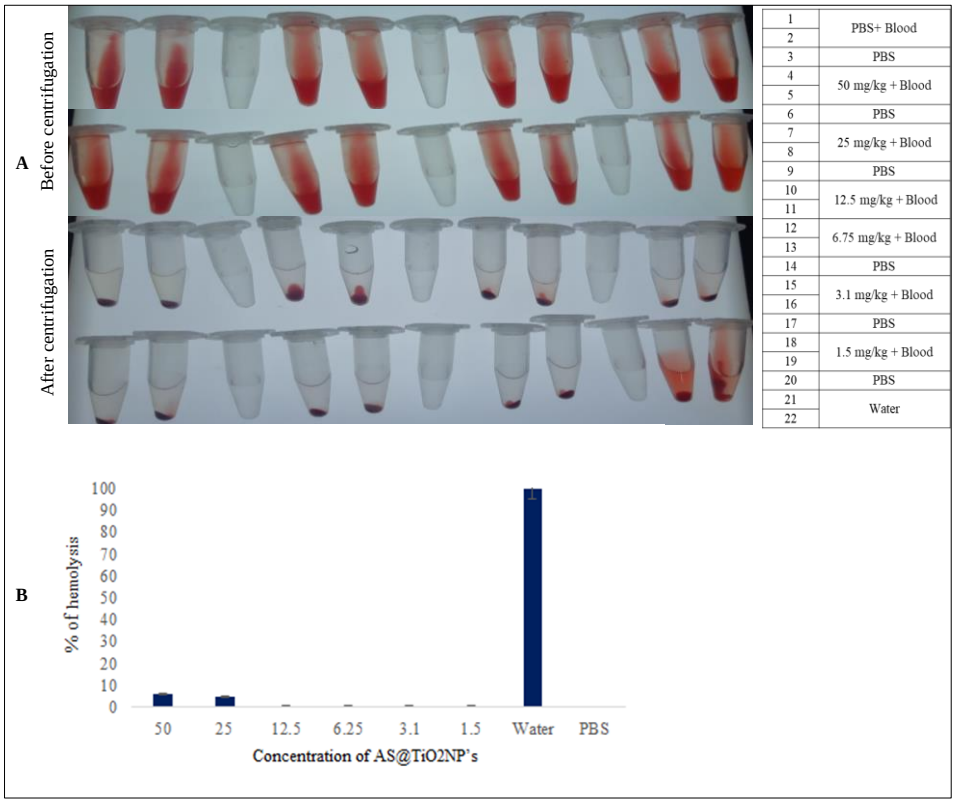


**Figure 12.** Biocompatibility nature of AS@$TiO_2$NP's. **(A)**The images represent the before and after treatment of AS@$TiO_2$NP's with a different concentration on RBCs. **(B)**% rate of RBCs.

*3.7. Cytotoxicity and antiproliferation of AS@$TiO_2$NP's against non-cancerous(3T3L1) and cancerous cell lines (MDAMB231).*

According to Behnam *et al.*, data claimed $TiO_2$NPs cause cell death or suppress cell proliferation [43]. The interactions between cells and the particles might lead to $TiO_2$ particle-mediated cell toxicity. Cell toxicity appears related to the surface properties of the $TiO_2$NPs, which are crucial to NP effectiveness. This is true even though the relationship between physicochemical parameters and potential toxicological effects is unclear. The ROS production and the biological impact of $TiO_2$NPs appear to be strongly influenced by the size and surface area of the particles [44].

Furthermore, Other studies show that $TiO_2$NPs have a negative charge and can attach to amino acids, specifically if their side chains contain -OH, -NH, or -NH2 [45]. $TiO_2$ NPs may therefore react with cell membrane proteins and facilitate interactions between particles and cells [46-48]. It appears that cell type, particle concentration, and surface characteristics all affect a cancer cell's cytotoxicity. The present investigation data revealed only 32.82% normal cell (3T3L1) inhibited at 320 µg/mL compared to the standard drug doxorubicin 28.27 µg/mL ($IC_{50}$) (Figure 13A, B & C).

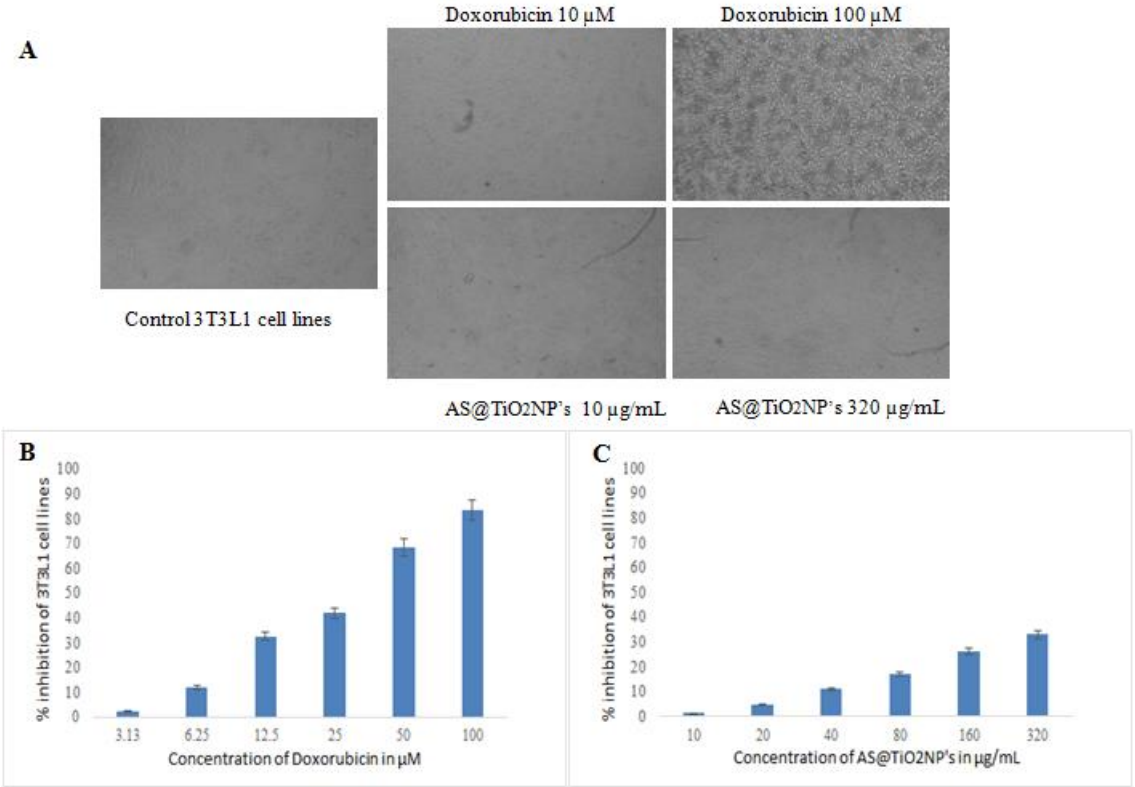


**Figure 13.** Cytotoxicity investigation of AS@$TiO_2$NP's. **(A)** Microscopic images of control and treated normal cell lines 3T3L1 in various concentrations of AS@$TiO_2$NP's and doxorubicin**. (B)**The picture depicts the % growth inhibition of normal cell lines 3T3L1.

MDA-MB-231 triple-negative breast cancer (TNBC) cell line is extremely aggressive, invasive, and poorly differentiated because it lacks the expression of the estrogen receptor (ER), the progesterone receptor (PR), and HER2 (human epidermal growth factor receptor 2). The AS@$TiO_2$NP'sshowed 70.14 µg/mL sufficient to inhibit the MDA-MB-231($IC_{50}$) cells with respect to doxorubicin at 17.69 µg/mL is required, and it is more potential drug in coming near future (Figures 14 A, B, & C).

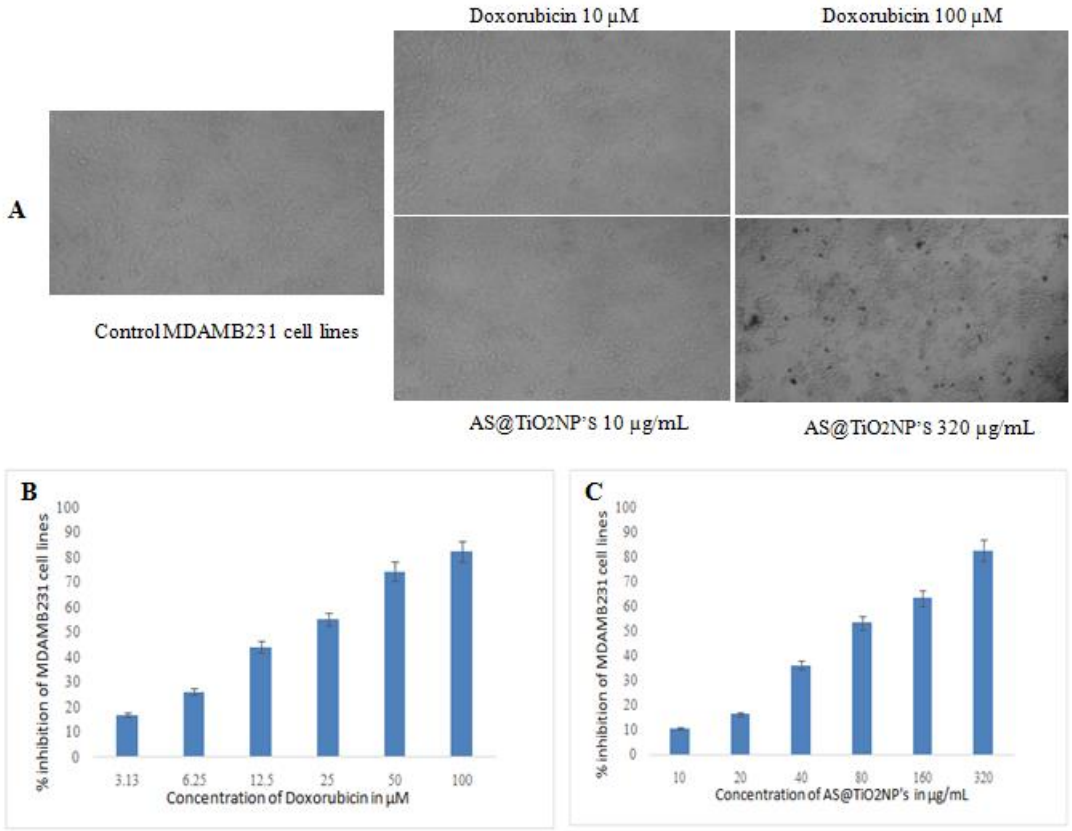


**Figure 14.** Cytotoxicity investigation of AS@$TiO_2$NP's.**(A)** Microscopic images of control and treated cancerous cell lines MDAMB231 in various concentrations of AS@$TiO_2$NP's and doxorubicin**. (B)**The picture depicts the % growth inhibition of cancerous cell lines MDAMB231.

## 4. Conclusions

In conclusion, a rapid, simple, and cost-effective green chemistry approach was established to synthesize bioactive compounds loaded with titanium dioxide nanoparticles. The AS@$TiO_2$NP was characterized using different spectral techniques like UV-Vis spectroscopy, FT-IR, XRD, DLX, SEM, and EDX analysis. The colloidal stability of AS@$TiO_2$NP's was amply studied with $p^H$, temperature, and salinity. The antibacterial potency of AS@$TiO_2$NP's was more lethal against Gram-negative pathogens than Gram-positive ones. The catalytic activity of AS@$TiO_2$NP's was more effective on the anionic dye methyl orange (MO) compared to the cationic dye methylene blue (MB).

Furthermore, nano drug prerequisite biocompatibility was investigated under hemostatic conditions, and the results revealed a high level of compatibility up to 25mg/Kg. The cytotoxicity of AS@$TiO_2$NP's was assessed on non-cancerous and cancerous triple-negative cell lines. The data indicated that the AS@$TiO_2$NP's could be a potential candidate for nanodrug preparation against dangerous human pathogens and industrial wastewater dye treatment.

## Funding

This research received no external funding.

## Acknowledgments

The authors would like to thank Skanda Life Sciences Pvt. Ltd., Bangalore, for providing timely and valuable assistance with cytotoxicity data.

## Conflicts of Interest

We declare that we have no conflict of interest.

## References

1. Yang, L.; Yang, L.; Ding, L.; Deng, F.; Luo, X. B.;& Luo, S. L. Principles for the application of nanomaterials in environmental pollution control and resource reutilization. In *Nanomaterials for the Removal of Pollutants and Resource Reutilization* **2019,** *2019*, 1-23,https://doi.org/10.1016/B978-0-12-814837-2.00001-9.
2. Yunus, I. S.; Harwin, Kurniawan, A.; Adityawarman, D.;& Indarto, A. Nanotechnologies in water and air pollution treatment. *Environmental Technology Reviews* **2012**, *1*, 136-148,https://doi.org/10.1080/21622515.2012.733966.
3. Choi, H.; Al-Abed, S. R.; Dionysiou, D. D.; Stathatos, E.; & Lianos, P. TiO2-based advanced oxidation nanotechnologies for water purification and reuse. *Sustainability science and engineering* **2010** , *2*, 229-254, https://doi.org/10.1016/S1871-2711(09)00208-6.
4. Akın, N.;& Mutlu Danacı, H. An investigation into the architectural use of nanotechnology in the context of the titanium dioxide. *Environmental Science and Pollution Research* **2021** , *28*, 64130-64136, https://doi.org/10.1007/s11356-021-15268-5.
5. Aswini, R.; Murugesan, S.; & Kannan, K. Bio-engineered TiO2 nanoparticles using Ledebouria revoluta extract: Larvicidal, histopathological, antibacterial and anticancer activity. *International Journal of Environmental Analytical Chemistry***2 021**, *101*, 2926-2936, https://doi.org/10.1080/03067319.2020.1718668.
6. Luo, Y. B.; Wang, X. L.; & Wang, Y. Z. Effect of TiO2 nanoparticles on the long-term hydrolytic degradation behavior of PLA. *Polymer degradation and stability* **2012**, *97*, 721-728, https://doi.org/10.1016/j.polymdegradstab.2012.02.011.
7. Álvarez, P. M.; Jaramillo, J.; Lopez-Pinero, F.; & Plucinski, P. K. Preparation and characterization of magnetic TiO2 nanoparticles and their utilization for the degradation of emerging pollutants in water. *Applied Catalysis B: Environmental* **2010**, *100*, 338-345, https://doi.org/10.1016/j.apcatb.2010.08.010.
8. Pelaez, M.; Armah, A.; Stathatos, E.; Falaras, P.; & Dionysiou, D. D. Visible light-activated NF-codoped TiO2 nanoparticles for the photocatalytic degradation of microcystin-LR in water. *Catalysis Today***2 009**, *144*, 19-25, https://doi.org/10.1016/j.cattod.2008.12.022.
9. Ananda, A. P.; Krishnamurthy, N. B.; Savitha, K. R.; & Nagendra, B. S. Biogenic synthesis of silver nanoparticles using Priva cordifolia leaf extract (PC@ AgNPs) a potent antioxidant, antibacterial and catalytic activity. *SN Applied Sciences* **2019**, *1*, 1-13, https://doi.org/10.1007/s42452-019-0818-4.
10. Donga, C.; Mishra, S. B.; Abd-El-Aziz, A. S.; & Mishra, A. K. Advances in graphene-based magnetic and graphene-based/TiO2 nanoparticles in the removal of heavy metals and organic pollutants from industrial wastewater. *Journal of Inorganic and Organometallic Polymers and Materials* **2021**, *31*, 463-480, https://doi.org/10.1007/s10904-020-01679-3.
11. Guilger-Casagrande, M.; Germano-Costa, T.; Pasquoto-Stigliani, T.; Fraceto, L. F.; & Lima, R. D. Biosynthesis of silver nanoparticles employing Trichoderma harzianum with enzymatic stimulation for the control of Sclerotinia sclerotiorum. *Scientific reports* **2019**, *9*, 1-9, https://doi.org/10.1038/s41598-019-50871-0.
12. Othman, A. M.; Elsayed, M. A.; Al-Balakocy, N. G.; Hassan, M. M.;& Elshafei, A. M. Biosynthesis and characterization of silver nanoparticles induced by fungal proteins and its application in different biological activities. *Journal of Genetic Engineering and Biotechnology* **2019**, *17*, 1-13,https://doi.org/10.1186/s43141-019-0008-1.
13. Burange, P. J.; Tawar, M. G.; Bairagi, R. A.; Malviya, V. R.; Sahu, V. K.; Shewatkar, S. N.; & Mamurkar, R. R. Synthesis of silver nanoparticles by using Aloe vera and Thuja orientalis leaves extract and their biological activity: a comprehensive review. *Bulletin of the National Research Centre* **2021**, *45*, 1-13, https://doi.org/10.1186/s42269-021-00639-2.
14. Urnukhsaikhan, E.; Bold, B. E.; Gunbileg, A.; Sukhbaatar, N.; & Mishig-Ochir, T. Antibacterial activity and characteristics of silver nanoparticles biosynthesized from Carduus crispus. *Scientific Reports* **2021**, *11*, 1-12, https://doi.org/10.1038/s41598-021-00520-2
15. Sousa, A.; Bradshaw, T. D.; Ribeiro, D.; Fernandes, E.; & Freitas, M. Pro-inflammatory effects of silver nanoparticles in the intestine. *Archives of Toxicology* **2022**, 1-21, https://doi.org/10.1007/s00204-022-03270-w.

16. Bhattacherjee, A.; Ghosh, T.; & Datta, A. Green synthesis and characterisation of antioxidant-tagged gold nanoparticle (X-GNP) and studies on its potent antimicrobial activity. *Journal of Experimental Nanoscience* **2018**, *13*, 50-61, https://doi.org/10.1080/17458080.2017.1407042.
17. Ahn, E. Y.; & Park, Y. Anticancer prospects of silver nanoparticles green-synthesized by plant extracts. *Materials Science and Engineering: C* **2020**, *116*, 111253, https://doi.org/10.1016/j.msec.2020.111253.
18. Sowmya, M.; Jinu, U.; Kannan, D.S.; Geetha, N.; Girija, S.; & Venkatachalam, P. Effect of silver nitrate and growth regulators on direct shoot organogenesis and *in vitro* flowering from internodal segment explants of *Alternanthera sessilis* L., *Biocatalysis and Agricultural Biotechnology* **2020**, *30*, 101855, https://doi.org/10.1016/j.bcab.2020.101855.
19. Rajput, S.; Kumar, D.; & Agrawal, V. Green synthesis of silver nanoparticles using Indian Belladonna extract and their potential antioxidant, anti-inflammatory, anticancer and larvicidal activities. *Plant cell reports* **2020**, *39*, 921-939, https://doi.org/10.1007/s00299-020-02539-7.
20. Prasad, H. N.; Ananda, A. P.; Sumathi, S.; Swathi, K.; Rakesh, K. J.; Jayanth, H. S.; & Mallu, P. Piperazine selenium nanoparticle (Pipe@ SeNP's): A futuristic anticancer contender against MDA-MB-231 cancer cell line. *Journal of Molecular Structure* **2022**, *1268*, 133683, https://doi.org/10.1016/j.molstruc.2022.133683.
21. Wang, L.; Zhang, H.; & Gao, Y. Effect of TiO2 nanoparticles on physical and mechanical properties of cement at low temperatures. *Advances in materials science and engineering* **2018**, *2018*, https://doi.org/10.1155/2018/8934689.
22. Kibasomba, P. M.; Dhlamini, S.; Maaza, M.; Liu, C. P.; Rashad, M. M.; Rayan, D. A.; & Mwakikunga, B. W. Strain and grain size of TiO2 nanoparticles from TEM, Raman spectroscopy and XRD: The revisiting of the Williamson-Hall plot method. *Results in Physics* **2018**, *9*, 628-635, https://doi.org/10.1016/j.rinp.2018.03.008.
23. Karisathan Sundararajan, N.; & Ammal, A. R. B. Improvement studies on emission and combustion characteristics of DICI engine fuelled with colloidal emulsion of diesel distillate of plastic oil, TiO2 nanoparticles and water. *Environmental Science and Pollution Research* **2018**, *25*, 11595-11613, https://doi.org/10.1007/s11356-018-1380-0.
24. AlQahtani, G. M.; AlSuhail, H. S.; Alqater, N. K.; AlTaisan, S. A.; Akhtar, S.; Khan, S. Q.; & Gad, M. M. Polymethylmethacrylate denture base layering as a new approach for the addition of antifungal agents. *Journal of Prosthodontics* **2022**, https://doi.org/10.1111/jopr.13561.
25. Othman, A. M.; Elsayed, M. A.; Al-Balakocy, N. G.; Hassan, M. M.; & Elshafei, A. M. Biosynthesis and characterization of silver nanoparticles induced by fungal proteins and its application in different biological activities. *Journal of Genetic Engineering and Biotechnology* **2019**, *17*, 1-13, https://doi.org/10.1186/s43141-019-0008-1.
26. Dhanya, C. S.; Paul, W.; Victor, S. P.; & Joseph, R. On improving the physiological stability of curcuminoids: Curcumininoid-silver nanoparticle complex as a better and efficient therapeutic agent. *Nano-Structures & Nano-Objects* **2021**, *25*, 100661, https://doi.org/10.1016/j.nanoso.2020.100661.
27. Bakhtiari-Sardari, A.; Mashreghi, M.; Eshghi, H.; Behnam-Rasouli, F.; Lashani, E.; & Shahnavaz, B. Comparative evaluation of silver nanoparticles biosynthesis by two cold-tolerant Streptomyces strains and their biological activities. *Biotechnology Letters* **2020**, *42*, 1985-1999, https://doi.org/10.1007/s10529-020-02921-1.
28. Sithole, R. K.; Machogo, L. F.; Moloto, M. J.; Gqoba, S. S.; Mubiayi, K. P.; Van Wyk, J.; & Moloto, N. One-step synthesis of Cu3N, Cu2S and Cu9S5 and photocatalytic degradation of methyl orange and methylene blue. *Journal of Photochemistry and Photobiology A: Chemistry* **2020**, *397*, 112577, https://doi.org/10.1016/j.jphotochem.2020.112577.
29. Wang, S.; Gao, H.; Fang, L.; Hu, Q.; Sun, G.; Chen, X.; & Yang, H. Synthesis of novel CQDs/CeO2/SrFe12O19 magnetic separation photocatalysts and synergic adsorption-photocatalytic degradation effect for methylene blue dye removal. *Chemical Engineering Journal Advances* **2021**, *6*, 100089, https://doi.org/10.1016/j.ceja.2021.100089.
30. Prasad, H. N.; Ananda, A. P.; Lohith, T. N.; Prabhuprasad, P.; Jayanth, H. S.; Krishnamurthy, N. B.; & Mallu, P. Design, synthesis, molecular docking and DFT computational insight on the structure of Piperazine sulfynol derivatives as a new antibacterial contender against superbugs MRSA. *Journal of Molecular Structure* **2022**, *1247*, 131333, https://doi.org/10.1016/j.molstruc.2021.131333.
31. Prasad, H. S. N.; Gaonkar, N. P.; Ananda, A. P.; Mukarambi, A.; Kumar, G. C.; Lohith, T. N.;& Beeregowda, N. Antibacterial Property of Schiff-based Piperazine against MRSA: Design, Synthesis, Molecular Docking, and DFT Computational Studies **2022**,*12*, https://doi.org/10.33263/LIANBS122.054.
32. Prasad, H. N.; Manukumar, H. M.; Karthik, C. S.; Mallesha, L.; & Mallu, P. A novel copper (II) PAmPiCaT complex (cPAmPiCaTc) as a biologically potent candidate: A contraption evidence against methicillin-resistant Staphylococcus aureus (MRSA) and a molecular docking proof. *Bioorganic & Medicinal Chemistry* **2019**, *27*, 841-850, https://doi.org/10.1016/j.bmc.2019.01.026.
33. Xu, J. M.; Song, S. T.; Tang, Z. M.; Jiang, Z. F.; Liu, X. Q.; Zhou, L.; & Liu, X. W. Predictive chemotherapy of advanced breast cancer directed by MTT assay *in vitro*. *Breast cancer research and treatment* **1999**, *53*, 77-85, https://doi.org/10.1023/A:1006122912146.

34. Mor, G. K.; Varghese, O. K.; Paulose, M.; Shankar, K.; & Grimes, C. A. A review on highly ordered, vertically oriented TiO2 nanotube arrays: Fabrication, material properties, and solar energy applications. *Solar Energy Materials and Solar Cells* **2006**, *90*, 2011-2075, https://doi.org/10.1016/j.solmat.2006.04.007.
35. Restrepo, C. V.; & Villa, C. C. Synthesis of silver nanoparticles, influence of capping agents, and dependence on size and shape: A review. *Environmental Nanotechnology, Monitoring & Management* **2021**, *15*, 100428, https://doi.org/10.1016/j.enmm.2021.100428.
36. Burley, S. K.; Bhikadiya, C.; Bi, C.; Bittrich, S.; Chen, L.; Crichlow, G. V.; & Zhuravleva, M. RCSB Protein Data Bank: powerful new tools for exploring 3D structures of biological macromolecules for basic and applied research and education in fundamental biology, biomedicine, biotechnology, bioengineering and energy sciences. *Nucleic acids research* **2021**, *49*, D437-D451,https://doi.org/10.1093/nar/gkaa1038.
37. Pc, J.; Marimuthu, T.; Devadoss, P.;& Kumar, S. M. Prevalence and measurement of anterior loop of the mandibular canal using CBCT: A cross sectional study. *Clinical implant dentistry and related research* **2018**, *20*, 531-534,https://doi.org/10.1111/cid.12609.
38. Haider, A. J.; AL–Anbari, R. H.; Kadhim, G. R.; & Salame, C. T. Exploring potential environmental applications of TiO2 nanoparticles. *Energy Procedia*, *119*, 332-345, 2017, https://doi.org/10.1016/j.egypro.2017.07.117.
39. Goutam, S. P.; Saxena, G.; Singh, V.; Yadav, A. K.; Bharagava, R. N.; & Thapa, K. B. Green synthesis of TiO2 nanoparticles using leaf extract of Jatropha curcas L. for photocatalytic degradation of tannery wastewater. *Chemical Engineering Journal* **2018**, *336*, 386-396,https://doi.org/10.1016/j.cej.2017.12.029.
40. Ravichandran, R.; Sundarrajan, S.; Venugopal, J. R.; Mukherjee, S.; & Ramakrishna, S. Applications of conducting polymers and their issues in biomedical engineering. *Journal of the Royal Society Interface* **2010**, *7*, S559-S579, https://doi.org/10.1098/rsif.2010.0120.
41. Gunavathi, C.; Sivasubramanian, K.; Keerthika, P.; & Paramasivam, C. A review on convolutional neural network based deep learning methods in gene expression data for disease diagnosis. *Materials Today: Proceedings* **2021**, *45*, 2282-2285, https://doi.org/10.1016/j.matpr.2020.10.263.
42. Zhang, X.; Manukumar, H. M.; Rakesh, K. P.; Karthik, C. S.; Prasad, H. N.; Swamy, S. N.;& Qin, H. L. Role of BP* C@ AgNPs in Bap-dependent multicellular behavior of clinically important methicillin-resistant Staphylococcus aureus (MRSA) biofilm adherence: a key virulence study. *Microbial pathogenesis* **2018**, *123*, 275-284, https://doi.org/10.1016/j.micpath.2018.07.025.
43. Kasner, S. E.; Swaminathan, B.; Lavados, P.; Sharma, M.; Muir, K.; Veltkamp, R.; & Burn, M. Rivaroxaban or aspirin for patent foramen ovale and embolic stroke of undetermined source: a prespecified subgroup analysis from the NAVIGATE ESUS trial. *The Lancet Neurology* **2018**, *17*, 1053-1060, https://doi.org/10.1016/S1474-4422(18)30319-3.
44. Jiang, W.; Kim, B.; Rutka, J. T.; & Chan, W. C; Nanoparticle-mediated cellular response is size-dependent. *Nature nanotechnology* **2008**, *3*, 145-150, https://doi.org/10.1038/nnano.2008.30.
45. Lagopati, N.; Evangelou, K.; Falaras, P.; Tsilibary, E. P. C.; Vasileiou, P. V.; Havaki, S.;& Gorgoulis, V. G. Nanomedicine: Photo-activated nanostructured titanium dioxide, as a promising anticancer agent. *Pharmacology & Therapeutics* **2021**, *222*, 107795, https://doi.org/10.1016/j.pharmthera.2020.107795.
46. Manjunatha, J. G; A surfactant enhanced graphene paste electrode as an effective electrochemical sensor for the sensitive and simultaneous determination of catechol and resorcinol. *Chemical Data Collections* **2020**, *25*, 100331,https://doi.org/10.1016/j.cdc.2019.100331.
47. Hareesha, N; & Manjunatha, J. G. Surfactant and polymer layered carbon composite electrochemical sensor for the analysis of estriol with ciprofloxacin. *Materials Research Innovations* **2020**, *24*, 349-362, https://doi.org/10.1080/14328917.2019.1684657.
48. Hareesha, N.; Manjunatha, J. G.; Raril, C., & Tigari, G.. Sensitive and selective electrochemical resolution of tyrosine with ascorbic acid through the development of electropolymerized alizarin sodium sulfonate modified carbon nanotube paste electrodes. *ChemistrySelect* **2019**, *4*, 4559-4567, https://doi.org/10.1002/slct.201900794.